YITP-SB-2024-31

Constraints on Strongly-Interacting Dark Matter from the James Webb Space Telescope

Peizhi Du,[1,2,*] Rouven Essig,[3,†] Bernard J. Rauscher,[4,‡] and Hailin Xu[3,§]

[1] *Laboratory of Spin Magnetic Resonance, School of Physical Sciences, Anhui Province Key Laboratory of Scientific Instrument Development and Application, University of Science and Technology of China, Hefei 230026, China*
[2] *New High Energy Theory Center, Department of Physics and Astronomy, Rutgers University, Piscataway, NJ 08854*
[3] *C.N. Yang Institute for Theoretical Physics, Stony Brook University, Stony Brook, NY, 11794, USA*
[4] *NASA Goddard Space Flight Center, Observational Cosmology Laboratory, Greenbelt, MD, 20771, USA*

Direct-detection searches for dark matter are insensitive to dark matter particles that have large interactions with ordinary matter, which are stopped in the atmosphere or the Earth's crust before reaching terrestrial detectors. We use "dark" calibration images taken with the HgCdTe detectors in the Near-Infrared Spectrograph (NIRSpec) on the James Webb Space Telescope (JWST) to derive novel constraints on sub-GeV dark matter candidates that scatter off electrons. We supplement the JWST analysis pipeline with additional masks to remove pixels with high-energy background events. For a 0.4% subcomponent of dark matter that interacts with an ultralight dark photon, we disfavor all previously allowed parameter space at high cross sections, and constrain some parameter regions for subcomponent fractions as low as ∼0.01%.

Introduction.—Although there is extensive evidence for dark matter (DM) from astrophysics and cosmology, its particle nature remains unknown. Direct-detection experiments provide an important probe of the interactions between DM and ordinary matter. Tremendous progress has been made in searching for ever weaker interactions, in particular also for sub-GeV DM masses [1–16]. In order to achieve sensitivity to low interaction cross sections, the experiments are typically placed underground to avoid cosmic rays and well-shielded to avoid radiogenic backgrounds. This means, however, that they are insensitive to DM that has strong[1] interactions with ordinary matter, which would be scattered or significantly slowed by the Earth's atmosphere, crust, and/or the shielding before reaching the detector. This effect is reflected as an upper limit on current direct-detection constraints [17–19].

Collider, accelerator, astrophysical, and cosmological data place stringent constraints on strongly-interacting DM, generally requiring interactions below a specific threshold [20–49]. The DM bounds depend sensitively on the DM mass and specific model and, for concreteness, we focus here on DM coupled to an ultralight dark-photon mediator, which is subject to many of the bounds applicable to millicharged particles. In particular, if this constitutes all of DM, constraints from the Cosmic Microwave Background (CMB) already rule out parameter space above the direct-detection upper limit [50, 51]. However, the CMB constraint vanishes if this constitutes only a sub-component of DM with fractional abundance $f_\chi \equiv \rho_\chi/\rho_{\rm DM} \lesssim 0.4\%$ [29], where $\rho_{\rm DM}$ is the total DM density. An allowed region above the ground-based direct-detection bounds then exists, see Fig. 1.

The unconstrained region can be probed by proposed accelerator- and collider-based experiments [52–58] or by leveraging the fact that the density can be significantly enhanced near the Earth's surface [59–68]. In addition, low-threshold balloon- and space-borne detectors can have reach beyond ground-based experiments due to the reduced or absent atmospheric shielding [19, 45, 69–74], provided they only have minimal shielding surrounding the detectors. For example, the DarkNESS mission proposes to use a Skipper-CCD on a satellite to probe the open region to very small fractional abundances f_χ [74].

In this letter, we show that *existing* space-based sensors can already probe the allowed region. In particular, we analyze "dark" images obtained with the Near Infrared Spectrograph (NIRSpec) on the James Webb Space Telescope (JWST) to place novel constraints on strongly-interacting sub-GeV DM. We simulate the expected DM signal assuming DM-electron interactions with an ultralight dark-photon mediator, including the detector shielding. Alongside the JWST image-processing pipeline, we develop a masking process to reduce high-energy events and their secondary impacts, while largely preserving the DM signal. Assuming the backgrounds after masking consist solely of Poisson-distributed dark current, we place constraints on the DM-electron cross-section for each DM mass based on the shape of the pixel charge distribution. Our results show that current JWST data can constrain a wide range of open parameter space between 1 MeV and 10 GeV DM masses for f_χ as low as ∼0.01%. The Supplemental Material (SM) contains additional details.

Dark matter signals at NIRSpec.—The JWST NIRSpec instrument features two detectors (NRS1 and NRS2) consisting of $Hg_{1-x}Cd_xTe$ with x = 0.3, which has a bandgap $E_{\rm gap} = 0.234\,{\rm eV}$. Each detector has

[1] "Strong" refers to the strength of the interaction between DM and ordinary matter, not to the strong force described by QCD.

2048 × 2048 pixels, including a 4-pixel wide frame of "reference pixels" on all sides that electronically mimic regular pixels, although they do not respond to light. The reference pixels are used within the JWST pipeline to remove correlated noise. Each pixel has an area of $18\,\mu\text{m} \times 18\,\mu\text{m}$ and a thickness of about $5\,\mu$m, corresponding to a detector mass of 0.05037 gram.

The analysis of the JWST data will depend on the properties of the DM candidate. For concreteness, we consider a fermionic DM particle χ coupled to an ultralight dark-photon mediator A' that is kinetically mixed with the ordinary photon [1, 19, 75, 76] (we leave other models to future work). The DM signal rate in the HgCdTe target is given by [1, 77–84]

$$\frac{\mathrm{d}R}{\mathrm{d}\ln E_e} = f_\chi \frac{\rho_\chi}{m_\chi} N_{\rm cell} \alpha \frac{\overline{\sigma}_e m_e^2}{\mu_{\chi e}^2} \int \frac{\mathrm{d}q}{q^2} E_e |F_{\rm DM}(q)|^2 \times \left| \frac{f_{\rm crys}(E_e, q)}{\epsilon(E_e, q)} \right|^2 \int_{v_\chi > v_{\rm min}} \mathrm{d}v_\chi \frac{1}{v_\chi} f_{\rm det}(v_\chi)\,, \quad (1)$$

where m_χ is the DM mass, m_e is the electron mass, $\mu_{\chi e}$ is the reduced DM-electron mass, $N_{\rm cell}$ is the number of unit cells in the crystal target, $f_{\rm crys}(E_e, q)$ is the crystal form factor, $v_{\rm min} = \frac{E_e}{q} + \frac{q}{2m_\chi}$, which is the minimum DM speed v_χ for the incoming DM particle to transfer energy E_e and momentum q to the target, $\rho_\chi = 0.3$ GeV/cm^3 is the local DM density [85, 86] (for more recent measurements, see e.g. [87–91]), and $f_{\rm det}(v)$ is the DM velocity distribution at the detector (see below). For the ultralight dark photon, we define the DM-electron reference cross section as $\overline{\sigma}_e \equiv 16\pi\alpha\alpha_D\epsilon^2\mu_{\chi e}^2/(\alpha m_e)^4$, where α (α_D) is the electromagnetic (dark) fine structure constant, and ϵ is the kinetic-mixing parameter. The DM form factor is $F_{\rm DM}(q) \equiv (\alpha m_e/q)^2$. We use `QEDark` [77, 92] to calculate the crystal form factor $f_{\rm crys}$ for both HgTe and CdTe. The factor $1/|\epsilon(E_e, q)|^2$ encodes screening effects, and we use the Lindhard formula to approximate the dielectric function $\epsilon(E_e, q)$ [93]. A more accurate determination of the scattering rate is in progress [94], while the evaluation used in this paper would overestimate the screening effect and result in a conservative estimation of the scattering rate. To convert E_e to the number of electron-hole pairs (denoted e^-) that are produced, Q, we use $Q(E_e) = 1 + \lfloor (E_e - E_{\rm gap})/\epsilon_{\rm eh} \rfloor$, for $E_e \geq E_{\rm gap}$, where the half-brackets represent the floor function, and the average energy needed to create an electron-hole pair is $\epsilon_{\rm eh} \sim 3E_{\rm gap}$ [95, 96]. Examples of the event rate are given in the SM. For each Q, we conservatively choose the lower rate between HgCd and CdTe.

JWST is located at Lagrange point L2, and we take its velocity the same as the Earth velocity in the galactic rest frame. We assume the standard halo model for the DM distribution in the galactic halo [86], where DM follows a Maxwell-Boltzmann velocity distribution truncated at galactic escape velocity. However, the velocity distribution of strongly-interacting DM at the detector $f_{\rm det}(v)$ can be drastically different due to the shielding surrounding the detector, as the DM can scatter and even be stopped by the shield for very large $\overline{\sigma}_e$. For the dark-photon mediator, the scattering off nuclei in the shield dominates the scattering, and we neglect the interactions with electrons in the shield [19]. The shielding consists of a camera housing, various mirrors, an optical bench, and other structures, and thus varies in different directions and is complicated to model precisely. Nevertheless, we can model it by assuming that the detector is surrounded on the front, top, left, and right by ∼20 mm of SiC, on the back by 12 mm Mo, and on the bottom (which contains the optical bench) by $\lesssim$25 mm of SiC [97, 98]. The 12 mm Mo-shield is roughly equivalent to 120 mm of SiC; we conservatively assume it cannot be penetrated by DM and reduce the incoming DM flux by a factor of two [99]. To determine $f_{\rm det}(v)$, we use `DaMaSCUS-CRUST` [100, 101] to perform Monte-Carlo simulations of DM passing through 20 mm of SiC. See SM for an example of the DM flux after detector shielding.

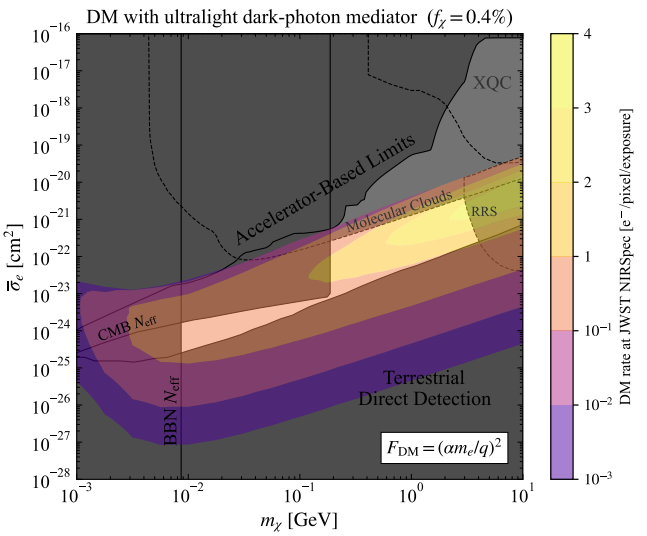


FIG. 1. The allowed parameter space for DM interacting with an ultralight dark photon for a fractional DM abundance of $f_\chi = 0.4\%$. The colored regions show the number of electrons created by DM-electron scattering in a NIRSpec HgCdTe detector in one full effective exposure (3559.7 seconds), divided by the number of pixels. The effects from the detector shielding are included. Dark gray regions with solid-line boundaries are bounds that are either independent or only scale mildly with f_χ [19–43], while light-gray regions with dashed-line boundaries are bounds that scale with f_χ [45–47].

Fig. 1 shows the number of electrons created by DM-electron scattering in a HgCdTe detector in one exposure (3559.7 seconds), divided by the number of pixels. The impact of the shielding is clearly visible for larger $\overline{\sigma}_e$.

JWST data and masks.—In this study, we consider the "full-frame-dark" images taken with the NRS2 NIRSpec

detector and an opaque filter that have the longest exposure (3574.3 seconds) (we checked the data from the NRS1 detector, but find that it naively is less suitable for a DM analysis, as we see patterns of noise across the image that seem difficult to model). The data are obtained from the Barbara A. Mikulski Archive for Space Telescopes [102]. We first study 20 datasets to design a preliminary analysis procedure. Ten datasets are from the first integration of an observation, which we found to have significantly less noise than the other ten datasets obtained from the second integration. We then discarded those images from the second integration and included an additional 20 first-integration datasets to further refine our analysis procedure. We finally applied this refined analysis procedure to all 30 first-integration datasets, which we list in the SM.

During a single integration of the dark image, the charges in each pixel are accumulating for ∼3574.3 seconds. However, during integration, the entire image is read out non-destructively 245 times each ∼14.6 seconds. Each readout will produce an image that contains a snapshot of the accumulated charges in each pixel at the time of readout; this image is called a "frame." After the full integration, the charges are discarded. The signal in each pixel is measured in digital numbers (DN), which can be converted to an inferred number of charges (N_e) after applying a gain factor correction [103].

The JWST image processing pipeline corrects pixel values and flags bad pixels [104]. We apply to our datasets the subset of the pipeline that does not affect a DM signal, which typically consists of $\lesssim$15 e^-. In addition, we develop custom masks to remove the impact of "high-energy" background events.

The JWST Image-Processing Pipeline. Starting with the uncalibrated files, we process each dataset through the JWST pipeline, which corrects the pixel values and flags their properties. From the pipeline, we use the following corrections: `superbias subtraction`, `reference pixel correction`, and `linearity correction`. We use the Improved Reference Sampling and Subtraction (`IRS`^{2}) readout scheme, which produces the lowest readout noise [105]. In addition, we remove from the subsequent analysis all pixels that have been flagged by the `saturation` step (∼1.4% of pixels), as these have DN values above the saturation threshold. We do not implement the `dark current subtraction` step, since this could remove part of a potential DM signal. In addition, we do not implement the `jump detection` step, since it could potentially remove some DM events; instead, we develop a similar but more conservative mask ourselves (see below).

To remove charges that accumulated before the start of the integration, we subtract from the DN value y_i for each pixel in each frame i ($i = 1, 2, \ldots, 245$), the DN value of the corresponding pixel in the first frame, y_1 (we suppress a pixel index). The total integrated DN for the full integration is then $y_{\rm int} \equiv y_{245} - y_1$, which corresponds to an effective exposure of ∼3559.7 seconds. The noise in $y_{\rm int}$ is then the superposition of the readout noise of two single frames, but we simply use "readout noise" to refer to the noise in $y_{\rm int}$. In Fig. 2, we show in gray the charge distribution for one dataset after applying the above JWST image-processing pipeline steps and converting DN to N_e by the gain factor. The charge distribution peaks near ∼15 e^-, with a long tail extending to very large charge values. Although the "dark" images are taken with an opaque filter, each image contains many cosmic-ray and radiogenic background events, in addition to a sizable dark current. We next apply custom masks to mitigate the high-energy backgrounds, while keeping potential DM events.

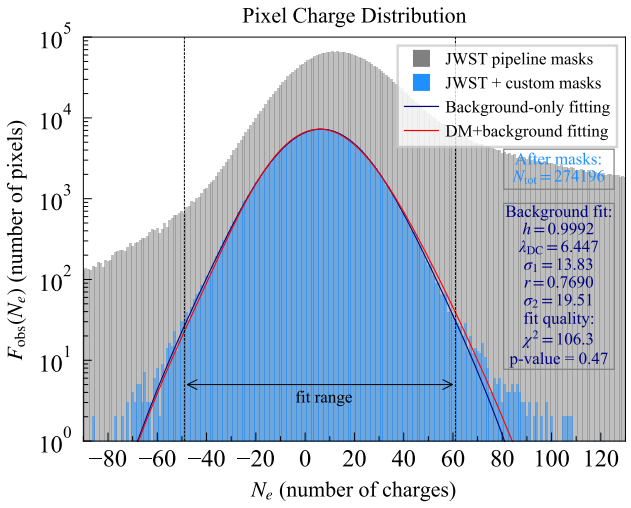


FIG. 2. Pixel charge distribution $F_{\rm obs}(N_e)$ in one full effective exposure of 3559.7 seconds for the dataset `obs_id: jw01121008001_02102_00001_nrs2` after applying a subset of the steps in the JWST image-processing pipeline (gray) and after applying our custom masks (blue) (see text for details). The navy curve is the fit to the data within the fit range (gray dashed lines) of the background model, corresponding to a Poisson distributed dark current with expectation value $\lambda_{\rm DC} = 6.447\ e^-$ and smeared by two Gaussian distributions (σ_1 and σ_2) to mimic the readout noise, with r being their relative contributions and h a normalization factor (see Eq. 2). The red curve shows the contribution of a DM signal together with a dark-current background, for $m_\chi = 1$ GeV and $\overline{\sigma}_e = 3.09 \times 10^{-22}$ cm^2, which is excluded at 95% CL.

Custom DM Masks. If a pixel has a sudden increase in DN value from one frame to the next frame that is larger than expected from a DM event plus a factor of few times the readout noise, then it very likely disturbed by a "high-energy" background event. We develop a `jump mask` to identify such pixels. In addition, high-energy events from cosmic rays or radiogenic backgrounds will deposit large amounts of charge in a set of connected pix-

Mask	Efficiency	Pixels left
`jump mask`	29.9(±0.7)%	69.0(±0.8)%
`cluster & halo mask`	40.3(±5.8)%	41.3(±4.4)%
`edge mask`	16.5(±1.3)%	34.5(±4.1)%
`hot-column mask`	50.5(±0.1)%	17.1(±2.2)%
`brightness mask`	68.2(±1.0)%	5.4(±0.8)%

TABLE I. The list of masks for mitigating backgrounds, together with the fraction of pixels removed ("efficiency") and the fraction of of pixels remaining (from a total number of 2048^2 pixels) after each mask. The errors in parentheses show the variation across the 30 datasets.

els, which we call "clusters". We find that these clusters are also surrounded by a "halo" of charges, which can extend in radius to $O(100)$ pixels (such combined clusters and halos are called "snowballs" in the JWST user community [106]). We will not study these here, but based on similar halos seen around high-energy events in SENSEI data [107], we hypothesize that the halos arise from Cherenkov radiation of high-velocity charged particles within the HgCdTe detectors [108, 109]. The jump mask is not efficient at removing the pixels within the halo, as they do not often have a large jump. We thus design a `cluster & halo mask` to reject pixels that are spatially correlated with a hot cluster. We use an `edge mask` to mask the edges of the image, since we find them to be less stable. Moreover, residual correlated noise remains after the `IRS`^{2} correction, appearing as "hot" columns in the image. We develop and implement a `hot-column mask` to account for this issue. Finally, we employ a `brightness mask` to remove pixels whose DN values are much larger than those expected by DM. Then we implement the gain correction to convert the DN of each pixel to N_e.

We next list the masks in detail. For each mask, we tried a range of cut values with the goal of removing much of the high-N_e tails of the pixel charge distribution shown in gray in Fig. 2.

- `jump mask:` This mask is inspired by the `jump detection` step in the JWST pipeline. We mask pixels whose value increases by > 60 DN between any two frames, i.e., which have $|y_i - y_{i-1}| > 60$ DN for at least one frame $i = 2, \ldots, 245$.
- `cluster & halo mask:` We divide the 2048×2048 pixels into 128×128 "mosaic pixels," each of which consists of 16×16 regular pixels. We then count the number of pixels flagged by the `jump mask` in each mosaic. If more than 70% (40%) of pixels in a given mosaic are flagged, we discard this mosaic along with the surrounding mosaics that are completely contained within a radius 3 (1) mosaics.
- `edge mask:` We mask 64 pixels (4 mosaic pixels) all around the edges of the image.
- `hot-column mask:` The image has 128 "mosaic columns". Each of them is 16 regular-pixels wide. The edge mask removes a total of 8 mosaic columns. For each of the remaining 120 mosaic columns, we sum the charge in the pixels that are not flagged by the pipeline or removed by the `jump mask` and that have 20 DN $< y_{\rm int} \leq 400$ DN. The upper bound of 400 DN is to ignore the few pixels with very large DN, which would contribute significantly to the summation but which are unlikely due to correlated noise. We then discard the 60 mosaic columns that have the largest summed charges.
- `brightness mask:` We mask any pixel with $|y_{\rm int}| > 150$ DN and a circular patch around it with a radius of 2 pixels.

After applying the above masks, we apply the gain correction to convert each pixels value in DN to the number of electrons, N_e. The gain factor of "good" pixels in NRS2 is on average 1.137 e^-/DN [103]; we remove pixels whose gain is < 0.6 e^-/DN. An example of the resulting charge distribution after the custom DM masks is shown in blue in Fig. 2, which looks approximately Gaussian. In particular, we see that much of the high-energy tail is removed. In addition, the `jump mask` also reduces the low-N_e tail significantly. We list the average mask efficiencies across all 30 datasets in Table I.

Dark matter constraints.—The observed charge distribution of the surviving pixels, $F_{\rm obs}(N_e)$, resembles the distribution expected from a Poisson distributed dark current (DC) convolved with readout noise. The DC values of the different datasets varies significantly (see SM), which is consistent with the variation in the peak of the charge distribution after the JWST pipeline steps (gray histogram in Fig. 2), and likely due to instrument instabilities. Nevertheless, a DM signal is expected to slightly skew the pixel charge distribution towards higher values of N_e, since DM will in some pixels deposit charges well above the average DC. To derive a constraint, we compare the measured pixel charge distribution within $|N_e - N_e^{\rm peak}| \leq 55$ ($N_e^{\rm peak}$ is the peak of the charge distribution after masks) with the one expected from a DM signal plus a DC signal. For a given m_χ and f_χ, the latter is given by

$$F(N_e) = N_{\rm tot}\, h \sum_n f(n; \overline{\sigma}_e, \lambda_{\rm DC}) g_{\rm read}(N_e, n), \tag{2}$$

$$g_{\rm read}(N_e, n) \equiv r\,{\rm Gauss}(N_e; n, \sigma_1) + (1-r){\rm Gauss}(N_e; n, \sigma_2)\ .$$

Here, $f(n; \overline{\sigma}_e, \lambda_{\rm DC})$ is the probability distribution function of the pixel charge distribution from the convolution of a DM signal and a Poisson distributed DC background with mean $\lambda_{\rm DC}$; $N_{\rm tot}$ is the number of surviving pixels; h accounts for the normalization factor of the distribution not necessarily being equal to $N_{\rm tot}$ (we find $0.998 < h \leq 1.000$ in the background-only fit of all datasets); $g_{\rm read}$ is the readout noise, modeled with two Gaussian distributions (since the readout noise differs between different pixels) indicated by ${\rm Gauss}(N_e; n, \sigma)$ with

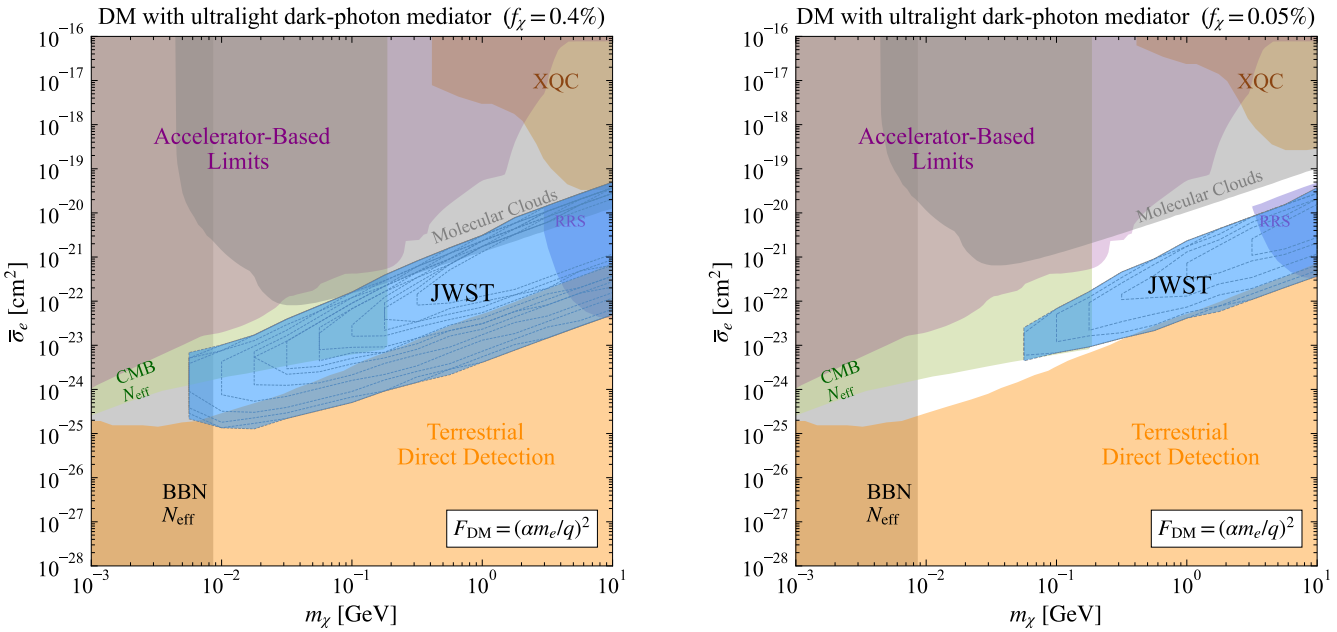


FIG. 3. **Blue regions** show the 95% CL constraints from 14 JWST NIRSpec dark images on the DM-electron scattering cross section $\overline{\sigma}_e$ versus the DM mass m_χ for DM interacting with ultralight dark-photon mediator, for a sub-component of DM with fractional abundance $f_\chi = 0.4\%$ (**left**) and $f_\chi = 0.05\%$ (**right**). The strongest bound is shaded blue, while the blue lines within show the excluded regions from the other datasets (in the right plot, not all 14 JWST datasets provide a constraint at 95% CL). Other limits are from [32, 36–38, 40, 43, 45, 46, 110].

mean n and variance σ; and the fractions r and $(1-r)$ ensure the probability density function $g_{\rm read}$ integrates to unity.

The background-only model is given by setting $\overline{\sigma}_e = 0$ in Eq. 2: $f(n; 0, \lambda_{\rm DC})$=Poisson$(n; \lambda_{\rm DC})$. We constrain our fit range to avoid the tails of the charge distribution, which likely contain non-DC backgrounds and pixels with poor noise performance, which we cannot adequately model. Fig. 2 shows the background fit curve in navy for one example dataset, together with the fit parameters (the fit range includes $\sim 99.8\%$ of surviving pixels). We note that the measured DC ($\lambda_{\rm DC} = 6.447\ e^-$) is comparable to the rates expected from DM-electron scattering via an ultralight mediator in the open parameter space for f_χ near 0.4%, see Fig. 1.

We calculate $\chi^2_{\rm fit}$ and p-value for the background model in each of the 30 datasets. The number of degrees of freedom is 106. We find that not all are fit well by the background model, likely due to an inadequate modeling of all noise sources. We thus select the 14 datasets with $\chi^2_{\rm fit} \leq 121$ (p-value> 0.15), for which the background model does provide a good fit. We show the charge distributions and the background fit for the other 13 datasets in the SM.

We next use the profile likelihood ratio test to derive constraint on $\overline{\sigma}_e$ for different m_χ and f_χ [111]. For a given m_χ and f_χ, we first obtain best-fit values for $(\overline{\sigma}_e, h, \lambda_{\rm DC}, \sigma_1, \sigma_2, r)$ that maximize the likelihood. We then scan over different values of $\overline{\sigma}_e$ while treating $(h, \lambda_{\rm DC}, \sigma_1, \sigma_2, r)$ as nuisance parameters to get the likelihood ratio with respect to the best-fit ones. We consider the one-sided test statistics q_μ to set the upper limit on $\overline{\sigma}_e$ [111]. In Fig. 3, we show the 95% confidence level (CL) constraints for $f_\chi = 0.4\%$ (left) and $f_\chi = 0.05\%$ (right), together with bounds from terrestrial direct-detection, accelerator-based searches, and cosmological bounds. The SM contains additional details about the statistics and bounds for other values of f_χ.

We see that the JWST NIRSpec data provide novel and important bounds on strongly-interacting DM, disfavoring the allowed parameter region for $f_\chi = 0.4\%$ for DM interacting with an ultralight dark photon. However, much viable parameter space remains for smaller f_χ, which can be probed by the proposed DarkNESS mission [74]. DarkNESS will use Skipper-CCDs, which have significantly lower and more stable noise than the NIRSpec detectors, the ability to count individual charges, and will have very little shielding, allowing for even larger cross sections to be probed.

We especially thank Megan Hott and Aman Singal for their help in calculating the DM-electron scattering form factor for HgCdTe. We thank Jialu Li, Weizhe Liu, Giacinto Piacquadio, Oren Slone, and Javier Tiffenberg for useful discussions. We thank Maurice te Plate for information on the NIRSpec detector shielding. PD is supported by National Natural Science Foundation of China (Grants No. T2388102) and was supported by DOE Grant DOE-SC0010008. RE acknowledges sup-

port from DOE Grant DE-SC0025309, Simons Investigator in Physics Award 623940, Heising-Simons Foundation Grant No. 79921, and Binational Science Foundation Grant No. 2020220. BR is supported by NASA as part of the James Webb Space Telescope Project. HX is supported by DOE Grant DE-SC0009854, Simons Investigator in Physics Award 623940, and Binational Science Foundation Grant No. 2020220.

* peizhi.du@rutgers.edu
† rouven.essig@stonybrook.edu
‡ Bernard.J.Rauscher@nasa.gov
§ hailin.xu@stonybrook.edu

[1] R. Essig, J. Mardon, and T. Volansky, Phys. Rev. D **85**, 076007 (2012), arXiv:1108.5383 [hep-ph].
[2] J. Tiffenberg, M. Sofo-Haro, A. Drlica-Wagner, R. Essig, Y. Guardincerri, S. Holland, T. Volansky, and T.-T. Yu (SENSEI), Phys. Rev. Lett. **119**, 131802 (2017), arXiv:1706.00028 [physics.ins-det].
[3] M. Crisler, R. Essig, J. Estrada, G. Fernandez, J. Tiffenberg, M. Sofo haro, T. Volansky, and T.-T. Yu (SENSEI), Phys. Rev. Lett. **121**, 061803 (2018), arXiv:1804.00088 [hep-ex].
[4] R. Agnese *et al.* (SuperCDMS), Phys. Rev. Lett. **121**, 051301 (2018), [erratum: Phys. Rev. Lett.122,no.6,069901(2019)], arXiv:1804.10697 [hep-ex].
[5] O. Abramoff *et al.* (SENSEI), Phys. Rev. Lett. **122**, 161801 (2019), arXiv:1901.10478 [hep-ex].
[6] A. Aguilar-Arevalo *et al.* (DAMIC), Phys. Rev. Lett. **123**, 181802 (2019), arXiv:1907.12628 [astro-ph.CO].
[7] L. Barak *et al.* (SENSEI), Phys. Rev. Lett. **125**, 171802 (2020), arXiv:2004.11378 [astro-ph.CO].
[8] Q. Arnaud *et al.* (EDELWEISS), Phys. Rev. Lett. **125**, 141301 (2020), arXiv:2003.01046 [astro-ph.GA].
[9] D. W. Amaral *et al.* (SuperCDMS), Phys. Rev. D **102**, 091101 (2020), arXiv:2005.14067 [hep-ex].
[10] I. Arnquist *et al.* (DAMIC-M), SciPost Phys. Proc. , 014 (2023).
[11] Z. Y. Zhang *et al.* (CDEX), Phys. Rev. Lett. **129**, 221301 (2022), arXiv:2206.04128 [hep-ex].
[12] R. Essig *et al.*, in *Snowmass 2021* (2022) arXiv:2203.08297 [hep-ph].
[13] I. Arnquist *et al.* (DAMIC-M), Phys. Rev. Lett. **130**, 171003 (2023), arXiv:2302.02372 [hep-ex].
[14] I. Arnquist *et al.* (DAMIC-M), Phys. Rev. Lett. **132**, 101006 (2024), arXiv:2307.07251 [hep-ex].
[15] P. Adari *et al.* (SENSEI), (2023), arXiv:2312.13342 [astro-ph.CO].
[16] M. F. Albakry *et al.* (SuperCDMS), (2024), arXiv:2407.08085 [hep-ex].
[17] G. D. Starkman, A. Gould, R. Esmailzadeh, and S. Dimopoulos, Phys. Rev. **D41**, 3594 (1990).
[18] G. Zaharijas and G. R. Farrar, Phys. Rev. **D72**, 083502 (2005), arXiv:astro-ph/0406531 [astro-ph].
[19] T. Emken, R. Essig, C. Kouvaris, and M. Sholapurkar, JCAP **09**, 070 (2019), arXiv:1905.06348 [hep-ph].
[20] X.-l. Chen, S. Hannestad, and R. J. Scherrer, Phys. Rev. **D65**, 123515 (2002), arXiv:astro-ph/0202496 [astro-ph].
[21] C. Dvorkin, K. Blum, and M. Kamionkowski, Phys. Rev. **D89**, 023519 (2014), arXiv:1311.2937 [astro-ph.CO].
[22] V. Gluscevic and K. K. Boddy, Phys. Rev. Lett. **121**, 081301 (2018), arXiv:1712.07133 [astro-ph.CO].
[23] S. D. McDermott, H.-B. Yu, and K. M. Zurek, Phys. Rev. **D83**, 063509 (2011), arXiv:1011.2907 [hep-ph].
[24] T. R. Slatyer, Phys. Rev. **D93**, 023527 (2016), arXiv:1506.03811 [hep-ph].
[25] A. D. Dolgov, S. L. Dubovsky, G. I. Rubtsov, and I. I. Tkachev, Phys. Rev. **D88**, 117701 (2013),

arXiv:1310.2376 [hep-ph].
[26] S. L. Dubovsky, D. S. Gorbunov, and G. I. Rubtsov, JETP Lett. **79**, 1 (2004), [Pisma Zh. Eksp. Teor. Fiz.79,3(2004)], arXiv:hep-ph/0311189 [hep-ph].
[27] W. L. Xu, C. Dvorkin, and A. Chael, Phys. Rev. **D97**, 103530 (2018), arXiv:1802.06788 [astro-ph.CO].
[28] Y. Ali-Haïmoud, J. Chluba, and M. Kamionkowski, Phys. Rev. Lett. **115**, 071304 (2015), arXiv:1506.04745 [astro-ph.CO].
[29] K. K. Boddy, V. Gluscevic, V. Poulin, E. D. Kovetz, M. Kamionkowski, and R. Barkana, Phys. Rev. D **98**, 123506 (2018), arXiv:1808.00001 [astro-ph.CO].
[30] H. Vogel and J. Redondo, JCAP **1402**, 029 (2014), arXiv:1311.2600 [hep-ph].
[31] S. Davidson, S. Hannestad, and G. Raffelt, JHEP **05**, 003 (2000), arXiv:hep-ph/0001179 [hep-ph].
[32] C. Creque-Sarbinowski, L. Ji, E. D. Kovetz, and M. Kamionkowski, Phys. Rev. D **100**, 023528 (2019), arXiv:1903.09154 [astro-ph.CO].
[33] C. Boehm, M. J. Dolan, and C. McCabe, JCAP **1308**, 041 (2013), arXiv:1303.6270 [hep-ph].
[34] A. Bhoonah, J. Bramante, F. Elahi, and S. Schon, Phys. Rev. **D100**, 023001 (2019), arXiv:1812.10919 [hep-ph].
[35] J. H. Chang, R. Essig, and S. D. McDermott, JHEP **09**, 051 (2018), arXiv:1803.00993 [hep-ph].
[36] A. A. Prinz *et al.*, Phys. Rev. Lett. **81**, 1175 (1998), arXiv:hep-ex/9804008 [hep-ex].
[37] G. Magill, R. Plestid, M. Pospelov, and Y.-D. Tsai, Phys. Rev. Lett. **122**, 071801 (2019), arXiv:1806.03310 [hep-ph].
[38] R. Acciarri *et al.* (ArgoNeuT), Phys. Rev. Lett. **124**, 131801 (2020), arXiv:1911.07996 [hep-ex].
[39] R. Harnik, R. Plestid, M. Pospelov, and H. Ramani, Phys. Rev. D **103**, 075029 (2021), arXiv:2010.11190 [hep-ph].
[40] R. Plestid, V. Takhistov, Y.-D. Tsai, T. Bringmann, A. Kusenko, and M. Pospelov, Phys. Rev. D **102**, 115032 (2020), arXiv:2002.11732 [hep-ph].
[41] A. Ball, G. Beauregard, J. Brooke, C. Campagnari, M. Carrigan, M. Citron, J. De La Haye, A. De Roeck, Y. Elskens, R. E. Franco, M. Ezeldine, B. Francis, M. Gastal, M. Ghimire, J. Goldstein, F. Golf, J. Guiang, A. Haas, R. Heller, C. S. Hill, L. Lavezzo, R. Loos, S. Lowette, G. Magill, B. Manley, B. Marsh, D. W. Miller, B. Odegard, F. R. Saab, J. Sahili, R. Schmitz, F. Setti, H. Shakeshaft, D. Stuart, M. Swiatlowski, J. Yoo, H. Zaraket, and H. Zheng, Phys. Rev. D **102**, 032002 (2020).
[42] L. Barak *et al.* (SENSEI), Phys. Rev. Lett. **133**, 071801 (2024), arXiv:2305.04964 [hep-ex].
[43] J. B. Muñoz and A. Loeb, Nature **557**, 684 (2018), arXiv:1802.10094 [astro-ph.CO].
[44] H. Liu, N. J. Outmezguine, D. Redigolo, and T. Volansky, Phys. Rev. D **100**, 123011 (2019), arXiv:1908.06986 [hep-ph].
[45] J. Rich, R. Rocchia, and M. Spiro, *New and Exotic Phenomena. Proceedings, 7th Moriond Workshop, Les Arcs, France, January 24-31, 1987*, Phys. Lett. **B194**, 173 (1987), [,221(1987)].
[46] M. S. Mahdawi and G. R. Farrar, JCAP **1810**, 007 (2018), arXiv:1804.03073 [hep-ph].
[47] A. Prabhu and C. Blanco, Phys. Rev. D **108**, 035035 (2023), arXiv:2211.05787 [hep-ph].
[48] D. F. G. Fiorillo and E. Vitagliano, Phys. Rev. Lett. **133**, 251004 (2024), arXiv:2404.07714 [hep-ph].
[49] P. Adshead, P. Ralegankar, and J. Shelton, JCAP **09**, 056 (2022), arXiv:2206.13530 [hep-ph].
[50] M. A. Buen-Abad, R. Essig, D. McKeen, and Y.-M. Zhong, Phys. Rept. **961**, 1 (2022), arXiv:2107.12377 [astro-ph.CO].
[51] D. V. Nguyen, D. Sarnaaik, K. K. Boddy, E. O. Nadler, and V. Gluscevic, Phys. Rev. D **104**, 103521 (2021), arXiv:2107.12380 [astro-ph.CO].
[52] K. J. Kelly and Y.-D. Tsai, Phys. Rev. D **100**, 015043 (2019), arXiv:1812.03998 [hep-ph].
[53] S. N. Gninenko, D. V. Kirpichnikov, and N. V. Krasnikov, Phys. Rev. D **100**, 035003 (2019), arXiv:1810.06856 [hep-ph].
[54] S. Foroughi-Abari, F. Kling, and Y.-D. Tsai, Phys. Rev. D **104**, 035014 (2021), arXiv:2010.07941 [hep-ph].
[55] S. Perez *et al.* (Oscura), JHEP **02**, 072 (2024), arXiv:2304.08625 [hep-ex].
[56] M. de Montigny, P.-P. A. Ouimet, J. Pinfold, A. Shaa, and M. Staelens, (2023), arXiv:2307.07855 [hep-ph].
[57] M. Kalliokoski, V. A. Mitsou, M. de Montigny, A. Mukhopadhyay, P.-P. A. Ouimet, J. Pinfold, A. Shaa, and M. Staelens, JHEP **04**, 137 (2024), arXiv:2311.02185 [hep-ph].
[58] Y.-D. Tsai, I. Hwang, R. Schmitz, M. Citron, K. Gunthoti, J. Steenis, H. Jeong, H. Moon, J. H. Yoo, and M. X. Liu, (2024), arXiv:2407.07142 [hep-ph].
[59] M. Pospelov and H. Ramani, Phys. Rev. D **103**, 115031 (2021), arXiv:2012.03957 [hep-ph].
[60] D. Budker, P. W. Graham, H. Ramani, F. Schmidt-Kaler, C. Smorra, and S. Ulmer, PRX Quantum **3**, 010330 (2022), arXiv:2108.05283 [hep-ph].
[61] A. Berlin, H. Liu, M. Pospelov, and H. Ramani, Phys. Rev. D **105**, 095028 (2022), arXiv:2110.06217 [hep-ph].
[62] J. H. Kim, I. S. Hwang, and J. H. Yoo, JHEP **05**, 031 (2021), arXiv:2102.11493 [hep-ex].
[63] F. Kling, J.-L. Kuo, S. Trojanowski, and Y.-D. Tsai, Nucl. Phys. B **987**, 116103 (2023), arXiv:2205.09137 [hep-ph].
[64] D. McKeen, M. Moore, D. E. Morrissey, M. Pospelov, and H. Ramani, Phys. Rev. D **106**, 035011 (2022), arXiv:2202.08840 [hep-ph].
[65] A. Berlin, H. Liu, M. Pospelov, and H. Ramani, Phys. Rev. D **109**, 075027 (2024), arXiv:2302.06619 [hep-ph].
[66] D. McKeen, D. E. Morrissey, M. Pospelov, H. Ramani, and A. Ray, Phys. Rev. Lett. **131**, 011005 (2023), arXiv:2303.03416 [hep-ph].
[67] M. Pospelov and A. Ray, JCAP **01**, 029 (2024), arXiv:2309.10032 [hep-ph].
[68] Y. Ema, M. Pospelov, and A. Ray, JHEP **07**, 094 (2024), arXiv:2402.03431 [hep-ph].
[69] D. Snowden-Ifft, S. Barwick, and P. Price, The Astrophysical Journal **364**, L25 (1990).
[70] D. P. Snowden-Ifft, S. W. Barwick, and P. B. Price, Astrophysical Journal Letters **364**, L25 (1990).
[71] B. D. Wandelt, R. Dave, G. R. Farrar, P. C. McGuire, D. N. Spergel, and P. J. Steinhardt, in *4th International Symposium on Sources and Detection of Dark Matter in the Universe (DM 2000)* (2000) pp. 263–274, arXiv:astro-ph/0006344.
[72] A. L. Erickcek, P. J. Steinhardt, D. McCammon, and P. C. McGuire, Phys. Rev. **D76**, 042007 (2007), arXiv:0704.0794 [astro-ph].
[73] J. S. Adams *et al.*, J. Low Temp. Phys. **199**, 1072 (2020),

arXiv:1908.09010 [astro-ph.IM].
[74] N. Saffold, P. M. Alpine, R. Essig, J. Estrada, T. Kim, D. Kubik, and M. F. Lembeck, PoS **TAUP2023**, 062 (2024).
[75] B. Holdom, Phys. Lett. **166B**, 196 (1986).
[76] P. Galison and A. Manohar, Phys. Lett. **136B**, 279 (1984).
[77] R. Essig, M. Fernandez-Serra, J. Mardon, A. Soto, T. Volansky, and T.-T. Yu, JHEP **05**, 046 (2016), arXiv:1509.01598 [hep-ph].
[78] Y. Hochberg, Y. Kahn, N. Kurinsky, B. V. Lehmann, T. C. Yu, and K. K. Berggren, Phys. Rev. Lett. **127**, 151802 (2021), arXiv:2101.08263 [hep-ph].
[79] S. Knapen, J. Kozaczuk, and T. Lin, Phys. Rev. D **104**, 015031 (2021), arXiv:2101.08275 [hep-ph].
[80] S. Knapen, J. Kozaczuk, and T. Lin, Phys. Rev. D **105**, 015014 (2022), arXiv:2104.12786 [hep-ph].
[81] S. M. Griffin, K. Inzani, T. Trickle, Z. Zhang, and K. M. Zurek, Phys. Rev. D **104**, 095015 (2021), arXiv:2105.05253 [hep-ph].
[82] Y. Kahn and T. Lin, Rept. Prog. Phys. **85**, 066901 (2022), arXiv:2108.03239 [hep-ph].
[83] T. Trickle, Phys. Rev. D **107**, 035035 (2023), arXiv:2210.14917 [hep-ph].
[84] C. E. Dreyer, R. Essig, M. Fernandez-Serra, A. Singal, and C. Zhen, Phys. Rev. D **109**, 115008 (2024), arXiv:2306.14944 [hep-ph].
[85] J. Lewin and P. Smith, Astroparticle Physics **6**, 87 (1996).
[86] D. Baxter *et al.*, Eur. Phys. J. C **81**, 907 (2021), arXiv:2105.00599 [hep-ex].
[87] R. Catena and P. Ullio, JCAP **08**, 004 (2010), arXiv:0907.0018 [astro-ph.CO].
[88] P. Salucci, F. Nesti, G. Gentile, and C. F. Martins, Astron. Astrophys. **523**, A83 (2010), arXiv:1003.3101 [astro-ph.GA].
[89] J. I. Read, J. Phys. G **41**, 063101 (2014), arXiv:1404.1938 [astro-ph.GA].
[90] P. F. de Salas and A. Widmark, Rept. Prog. Phys. **84**, 104901 (2021), arXiv:2012.11477 [astro-ph.GA].
[91] S. H. Lim, E. Putney, M. R. Buckley, and D. Shih, JCAP **01**, 021 (2025), arXiv:2305.13358 [astro-ph.GA].
[92] "`QEDark`," `https://github.com/tientienyu/QEdark`.
[93] M. Dressel and G. Grüner, *Electrodynamics of Solids: Optical Properties of Electrons in Matter* (Cambridge University Press, 2002).
[94] C. E. Dreyer, R. Essig, M. Fernandez-Serra, M. Hott, and A. Singal, (to appear).
[95] C. A. Klein, Journal of Applied Physics **39**, 2029 (1968).
[96] R. C. Alig, S. Bloom, and C. W. Struck, Phys. Rev. B **22**, 5565 (1980).
[97] P. Jakobsen, P. Ferruit, C. Alves de Oliveira, S. Arribas, G. Bagnasco, R. Barho, T. Beck, S. Birkmann, T. Böker, A. Bunker, S. Charlot, P. de Jong, G. de Marchi, R. Ehrenwinkler, M. Falcolini, R. Fels, M. Franx, D. Franz, M. Funke, G. Giardino, X. Gnata, W. Holota, K. Honnen, P. Jensen, M. Jentsch, T. Johnson, D. Jollet, H. Karl, G. Kling, J. Köhler, M. G. Kolm, N. Kumari, M. Lander, R. Lemke, M. López-Caniego, N. Lützgendorf, R. Maiolino, E. Manjavacas, A. Marston, M. Maschmann, R. Maurer, B. Messerschmidt, S. Moseley, P. Mosner, D. Mott, J. Muzerolle, N. Pirzkal, J. F. Pittet, A. Plitzke, W. Posselt, B. Rapp, B. Rauscher, T. Rawle, H. W. Rix, A. Rödel, P. Rumler, E. Sabbi, J. C. Salvignol, T. Schmid, M. Sirianni, C. Smith, P. Strada, M. te Plate, J. Valenti, T. Wettemann, T. Wiehe, M. Wiesmayer, C. Willott, R. Wright, P. Zeidler, and C. Zincke, A&A **661**, A80 (2022).
[98] S. M. Birkmann, G. Giardino, M. Sirianni, P. Ferruit, B. J. Rauscher, C. Alves de Oliveira, T. Böker, N. Kumari, N. Lützgendorf, E. Manjavacas, C. Proffitt, T. Rawle, M. te Plate, and P. Zeidler, Proc SPIE **12180**, 101 (2022).
[99] These estimates of materials surrounding the NIRSpec detector were informed, in part, by private conversations with the NIRSpec System Engineer, Maurice te Plate,.
[100] T. Emken and C. Kouvaris, "DaMaSCUS-CRUST v1.1, [ascl:1803.001] Available at https://github.com/temken/ and archived under [DOI: 10.5281/zenodo.2846401]," (2018-2019).
[101] T. Emken and C. Kouvaris, Phys. Rev. **D97**, 115047 (2018), arXiv:1802.04764 [hep-ph].
[102] "Barbara A. Mikulski Archive for Space Telescopes," `https://mast.stsci.edu/portal/Mashup/Clients/Mast/Portal.html`.
[103] JWST User Documentation: `https://jwst-docs.stsci.edu/jwst-near-infrared-spectrograph/nirspec-instrumentation/nirspec-detectors/nirspec-detector-performance`,.
[104] H. Bushouse, J. Eisenhamer, N. Dencheva, J. Davies, P. Greenfield, J. Morrison, P. Hodge, B. Simon, D. Grumm, M. Droettboom, E. Slavich, M. Sosey, T. Pauly, T. Miller, R. Jedrzejewski, W. Hack, D. Davis, S. Crawford, D. Law, K. Gordon, M. Regan, M. Cara, K. MacDonald, L. Bradley, C. Shanahan, W. Jamieson, M. Teodoro, and T. Williams, "JWST Calibration Pipeline," Zenodo (2023).
[105] B. J. Rauscher, R. G. Arendt, D. J. Fixsen, M. A. Greenhouse, M. Lander, D. Lindler, M. Loose, S. H. Moseley, D. B. Mott, Y. Wen, D. V. Wilson, and C. Xenophontos, Publications of the Astronomical Society of the Pacific **129**, 105003 (2017).
[106] JWST User Documentation: `https://jwst-docs.stsci.edu/depreciated-jdox-articles/data-artifacts-and-features/snowballs-and-shower-artifacts`,.
[107] L. Barak, I. M. Bloch, M. Cababie, G. Cancelo, L. Chaplinsky, F. Chierchie, M. Crisler, A. Drlica-Wagner, R. Essig, J. Estrada, E. Etzion, G. F. Moroni, D. Gift, S. Munagavalasa, A. Orly, D. Rodrigues, A. Singal, M. S. Haro, L. Stefanazzi, J. Tiffenberg, S. Uemura, T. Volansky, and T.-T. Yu (SENSEI Collaboration), Phys. Rev. Lett. **125**, 171802 (2020).
[108] P. Du, D. Egana-Ugrinovic, R. Essig, and M. Sholapurkar, Phys. Rev. X **12**, 011009 (2022).
[109] P. Du, D. Egaña Ugrinovic, R. Essig, and M. Sholapurkar, JHEP **01**, 164 (2024), arXiv:2310.03068 [hep-ph].
[110] A. Ball *et al.*, Phys. Rev. D **102**, 032002 (2020), arXiv:2005.06518 [hep-ex].
[111] G. Cowan, K. Cranmer, E. Gross, and O. Vitells, Eur. Phys. J. C **71**, 1554 (2011), [Erratum: Eur.Phys.J.C 73, 2501 (2013)], arXiv:1007.1727 [physics.data-an].